ROTOR-DYNAMIC CHARACTERISTIC EVALUATION OF INTERIOR PERMANENT MAGNET MOTOR USING FINITE ELEMENT METHOD

Hilman Syaeful Alam [a,*], Pudji Irasari [b]

[a]Technical Implementation Unit for Instrumentation Development, Indonesian Institute of Sciences,
Jl. Sangkuriang Komplek LIPI Gedung 30 Bandung, 40135, Indonesia.
[b]Research Centre for Electrical Power and Mechatronics, Indonesian Institute of Sciences,
Jl. Sangkuriang Komplek LIPI Gedung 20 Lantai 2 Bandung, 40135, Indonesia.

Abstract

Dynamic characteristics of a critical speed of the rotor components at interior permanent magnet motor were evaluated using one-dimensional (1D) and three-dimensional (3D) finite element methods. Critical speed of the rotor wasinvestigated in the Campbell diagram, which shows the relationship between natural frequency and rotational velocity of the system when the motor is not in operation. The 1D finite element analysis shows that there are two modes which are close to the design frequency of 300 Hz i.e. mode 1 and 2. However the critical rotational velocity in both modes are still far above the maximum velocity design of 6,000 rpm. Validation using 3D finite element analysis demonstrated that all modes were still above the designed frequency and did not find any critical speed below 6,000 rpm. It can be concluded that the critical speed of the rotor of IPM motor is still outside the system resonance region, and can be operated safely.

Keywords: natural frequency, campbell diagram, interior permanent magnet motor, finite element method.

I. INTRODUCTION

Interior permanent magnet (IPM) motor is one of electric motor type, which is widely applied in the compact system for its several advantages: lightweight, small size, simple mechanical construction, easy maintenance, high reliability as well as high energy to volume ratio [1-5]. One of the problems in designing the rotating machinery including IPM motors is the vibration, because the vibration is usually a direct cause of the component damage. Every spinning rotor has some vibration, at least a once-per-revolution frequency component (1st order) therefore it is impossible to make any rotor perfectly mass balanced. Rotor-dynamic analysis is essential for quantifying safe upper limits of allowable vibration levels by analyzing the critical speed of the system which is very useful. It can provide information about the resonance region of the system and can be used as a standard to monitor the possibility of harmful, due to damage of the components. In addition, it is very useful for designers in understanding the relationship between the selection of design schemes including the shaft size, bearing properties, housing stiffness and machine stability [6].

There are two methods which are often adopted to deal with rotor dynamic problem. One is the transfer matrix method, such as Riccati transfer matrix method and the other is the finite element method (FEM), which has higher numerical stability but need more storage space of the computer. Both methods are widely used to solve the rotor dynamic problem. The former method divides the system into several parts after it gets the lumped mass model, such as the disk, the shaft and the bearing. Then it establishes the relation of the state vectors between the both ends of the cross-section and use the continuity conditions to obtain the relation between the state vectors in any cross section and the initial one. The latter method, namely FEM, was not adopted to analyze rotor dynamic problem until 1970s.The key idea of the FEM is to transform the infinite DOF (Degrees of Freedom) problem into a finite number of DOF, and then solve it. As the computer technology develops, the FEM become very popular to analyze mechanical problems, not just the rotor dynamic [7].

*Corresponding Author. Tel.: +62-81394297528
E-mail: alam_hilman@yahoo.com

The FEM has several advantages such as reduction of time when solving complex equation system. In addition, it can be applied by the software and can be widely applied in solving problems in engineering field for high accuracy and flexibility [8]. Some previous research have been used finite element to evaluate the dynamic characteristics of the rotor shaft system for some applications, such as: main shaft system in a hydro-turbine [7], gas turbine rotor [8], rotating structures [9], rotor-shaft system for evaluating hydro-dynamic action in journal bearings [10], and induction motors [11], and the rotor deflection of permanent magnet (PM) generator [12]. In this study, the dynamic characteristic of the rotor is evaluated using finite element method, in order to determine the existence of a critical speed and safe upper limits of allowable vibration levels of IPM motors, so it can be used as a reference for dynamic analysis and a foundation for the design or improvement.

II. MATERIALS AND METHODS

The dynamic characteristic of the rotor was evaluated using finite element method by analyzing the critical speed based on the Campbell diagram which represents the relationship between the natural frequencies and the rotational velocity of the system. 1D finite element analysis is conducted numerically based on the development of the Lagrange equations and the effects of unbalanced mass and bearing influence are neglected. Then, the results of analysis are validated using ANSYS, a commercially software based on three 3D finite element analysis. The main components of rotor are the shaft, bearing and permanent magnet along with the crank which is modeled simply as a disk, shown in Figure 1.

To determine the dynamic characteristics of the rotor, the calculation of the kinetic energy T is required to characterize disk, shaft and unbalanced mass. In addition, the strain energy U is employed to characterize the shaft. Force on the bearing as the action force on the shaft is used to calculate the virtual work δW due to an external force. The general equation to evaluate the dynamic characteristics of the rotor can be modeled using Lagrange equation as follows [15]:

$$\frac{d}{dt}\left(\frac{\partial T}{\partial q_i}\right) - \frac{\partial T}{\partial q_i} + \frac{\partial U}{\partial q_i} = Fq_i \qquad (1)$$

where $N(1 \leq i \leq N)$ is the number degree of freedom, q_i are generalized independent coordinates, Fq_i are generalized forces, and denotes differentiation with respect to time t.
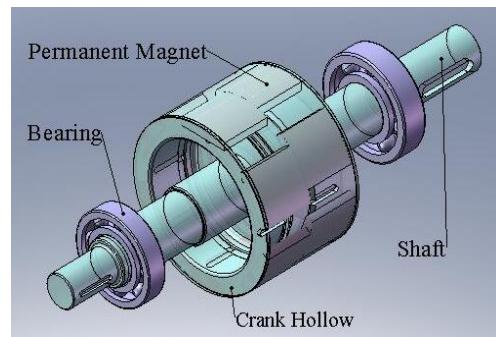

Figure 1. Rotor components of IPM motors

A. 1D Finite Element

In 1D finite element, shaft is modeled as a beam which has a constant circular cross-section. If the element has two nodal, it will form the 8-order matrix. Each of the nodal has 4 degrees of freedom: 2 displacements and 2 slopes in both x-y plane and y-z planes (Figure 2), therefore nodal displacement vector can be written in the equation [15]:

$$\delta = [u_1, w_1, \theta_1, \psi_1, u_2, w_2, \theta_2, \psi_2]^T \qquad (2)$$

The relationship between displacement and slope are:

$$\theta = \frac{\delta w}{\delta y} \qquad (3)$$

$$\psi = -\frac{\delta u}{\delta y} \qquad (4)$$

Displacements δu and δw in accordance with movements in the X and Z directions written by the equation:

$$\delta u = [u_1, \psi_1, u_2, \psi_2]^T \qquad (5)$$

$$\delta w = [w_1, \theta_1, w_2, \theta_2]^T \qquad (6)$$

Displacements in the finite element are formed from:

$$u = N_1(y)\delta u \qquad (7)$$

$$w = N_2(y)\delta w \qquad (8)$$

$N_1(y)$ and $N_2(y)$ are the function of displacements for the beam that are subjected to bending loads:
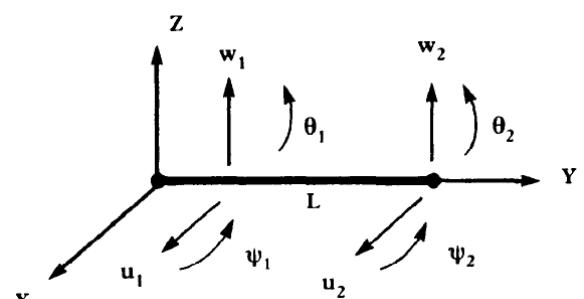

Figure 2. Modeling of one dimensional (1D) rotor [15]

$$N_1(y) = \left[1 - \frac{3y^2}{L^2} + \frac{2y^3}{L^3}; -y + \frac{2y^2}{L} - \frac{y^3}{L^2}; \frac{3y^2}{L^2} - \frac{2y^3}{L^3}; \frac{y^2}{L} - \frac{y^3}{L^2}\right] \tag{9}$$

$$N_2(y) = \left[1 - \frac{3y^2}{L^2} + \frac{2y^3}{L^3}; y - \frac{2y^2}{L} + \frac{y^3}{L^2}; \frac{3y^2}{L^2} - \frac{2y^3}{L^3}; -\frac{y^2}{L} + \frac{y^3}{L^2}\right] \tag{10}$$

Kinetic energy of the shaft can be calculated as:

$$T = \frac{\rho S}{2} \int_0^L \left[\delta \dot{u}^T N_1{}^T N_1 \delta \dot{u} + \delta \dot{w}^T N_2{}^T N_2 \delta \dot{w}\right] dy + \frac{\rho I}{2} \int_0^L \left[\delta \dot{u}^T \frac{dN_1{}^T}{dy} \frac{dN_1}{dy} \delta \dot{u} + \delta \dot{w}^T \frac{dN_2{}^T}{dy} \frac{dN_2}{dy} \delta \dot{w}\right] dy - 2\rho I \Omega \int_0^L \delta \dot{u}^T \frac{dN_1{}^T}{dy} \frac{dN_2}{dy} \delta w dy + \rho I L \Omega^2 \tag{11}$$

where ρ is the mass per unit volume, S is the cross sectional area of the beam, and I is the area moment of inertia of the beam cross section about the neutral axis, L is the length of element and Ω is the angular velocity.

Substitution of equation (9) and (10) into equation (11), then:

$$T = \frac{1}{2}\delta \dot{u}^T M_1 \delta \dot{u} + \frac{1}{2}\delta \dot{w}^T M_2 \delta \dot{w} + \frac{1}{2}\delta \dot{u}^T M_3 \delta \dot{u} + \frac{1}{2}\delta \dot{w}^T M_4 \delta \dot{w} + \Omega \delta \dot{u}^T M_5 \delta w + \rho I L \Omega^2 \tag{12}$$

M_1 and M_2 are the classical mass matrix, M_3 and M_4 are generated due to a secondary effect of rotor inertia, and M_5 is generated due to gyroscopic. By applying the Lagrange equation, then:

$$\frac{d}{dt}\left(\frac{\partial T}{\partial \dot{\delta}}\right) - \frac{\partial T}{\partial \delta} = (M + M_s)\ddot{\delta} + C\dot{\delta} \tag{13}$$

where M and M_s are obtained from M_1, M_2, M_3, M_4 and C from M_5, thus:

$$M = \frac{\rho S L}{420} \begin{bmatrix} 156 & 0 & 0 & -22L & 54 & 0 & 0 & 13L \\ 0 & 156 & 22L & 0 & 0 & 54 & -13L & 0 \\ 0 & 22L & 4L^2 & 0 & 0 & 13L & -3L^2 & 0 \\ -22L & 0 & 0 & 4L^2 & -13L & 0 & 0 & -3L^2 \\ 54 & 0 & 0 & -13L & 156 & 0 & 0 & 22L \\ 0 & 54 & 13L & 0 & 0 & 156 & -22L & 0 \\ 0 & -13L & -3L^2 & 0 & 0 & -22L & 4L^2 & 0 \\ 13L & 0 & 0 & -3L^2 & 22L & 0 & 0 & 4L^2 \end{bmatrix} \tag{14}$$

$$M_s = \frac{\rho I}{30L} \begin{bmatrix} 36 & 0 & 0 & -3L & -36 & 0 & 0 & -3L \\ 0 & 36 & 3L & 0 & 0 & -36 & 3L & 0 \\ 0 & 3L & 4L^2 & 0 & 0 & -3L & -L^2 & 0 \\ -3L & 0 & 0 & 4L^2 & 3L & 0 & 0 & -L^2 \\ -36 & 0 & 0 & 3L & 36 & 0 & 0 & 3L \\ 0 & -36 & -3L & 0 & 0 & 36 & -3L & 0 \\ 0 & 3L & --L^2 & 0 & 0 & -3L & 4L^2 & 0 \\ -3L & 0 & 0 & -L^2 & 3L & 0 & 0 & 4L^2 \end{bmatrix} \tag{15}$$

$$C = \frac{\rho I \Omega}{15L} \begin{bmatrix} 36 & 0 & 0 & -3L & -36 & 0 & 0 & -3L \\ 0 & 36 & 3L & 0 & 0 & -36 & 3L & 0 \\ 0 & 3L & 4L^2 & 0 & 0 & -3L & -L^2 & 0 \\ -3L & 0 & 0 & 4L^2 & 3L & 0 & 0 & -L^2 \\ -36 & 0 & 0 & 3L & 36 & 0 & 0 & 3L \\ 0 & -36 & -3L & 0 & 0 & 36 & -3L & 0 \\ 0 & 3L & --L^2 & 0 & 0 & -3L & 4L^2 & 0 \\ -3L & 0 & 0 & -L^2 & 3L & 0 & 0 & 4L^2 \end{bmatrix} \tag{16}$$

Strain energy on the shaft can be calculated by the equation:

$$U = \frac{EI}{2} \int_0^L \left[\delta u^T \frac{d^2N_1{}^T}{dy^2} \frac{d^2N_1}{dy^2} \delta u + \delta w^T \frac{d^2N_2{}^T}{dy^2} \frac{d^2N_2}{dy^2} \delta w\right] dy$$

$$+ \frac{F_0}{2} \int_0^L \left[\delta u^T \frac{dN_1{}^T}{dy} \frac{dN_1}{dy} \delta u + \delta w^T \frac{dN_2{}^T}{dy} \frac{dN_2}{dy} \delta w\right] dy \tag{17}$$

Then, after integration:

$$U = \frac{1}{2}\delta u^T K_1 \delta u + \frac{1}{2}\delta w^T K_2 \delta w + \frac{1}{2}\delta u^T K_3 \delta u + \frac{1}{2}\delta w^T K_4 \delta w \tag{18}$$

where K_1 and K_2 are the classical stiffness matrix (K_c), K_3 and K_4 are the matrix due to the axial force (K_f).

The effect of shear force can be calculated by the equation:

$$a = \frac{12EI}{GS_rL^2} \tag{19}$$

with shear modulus:

$$G = \frac{E}{2(1+v)} \tag{20}$$

where v is the Poissons ratio and E is Young's modulus of the material. Then by applying Eq. (17) to the Lagrange equation:

$$\frac{\partial U}{\partial \delta} = K\delta \tag{21}$$

$$K = K_C + K_F \tag{22}$$

where K_C dan K_F, can be calculated

$$K_C = \frac{EI}{(1+a)L^3}\begin{bmatrix} 12 & 0 & 0 & -6L & -12 & 0 & 0 & -6L \\ 0 & 12 & 6L & 0 & 0 & -12 & 6L & 0 \\ 0 & 6L & (4+a)L^2 & 0 & 0 & -6L & (2-a)L^2 & 0 \\ -6L & 0 & 0 & (4+a)L^2 & 6L & 0 & 0 & (2-a)L^2 \\ -12 & 0 & 0 & 6L & 12 & 0 & 0 & 6L \\ 0 & -12 & -6L & 0 & 0 & 12 & -6L & 0 \\ 0 & 6L & (2-a)L^2 & 0 & 0 & -6L & (4+a)L^2 & 0 \\ -6L & 0 & 0 & (2-a)L^2 & 6L & 0 & 0 & (4+a)L^2 \end{bmatrix} \tag{23}$$

$$K_F = \frac{F}{30L}\begin{bmatrix} 36 & 0 & 0 & -3L & -36 & 0 & 0 & -3L \\ 0 & 36 & 3L & 0 & 0 & -36 & 3L & 0 \\ 0 & 3L & 4L^2 & 0 & 0 & -3L & (-L^2) & 0 \\ -3L & 0 & 0 & 4L^2 & 3L & 0 & 0 & -L^2 \\ -36 & 0 & 0 & 3L & 36 & 0 & 0 & 3L \\ 0 & -36 & -3L & 0 & 0 & 36 & -3L & 0 \\ 0 & 3L & -L^2 & 0 & 0 & -3L & 4L^2 & 0 \\ -3L & 0 & 0 & -L^2 & 3L & 0 & 0 & 4L^2 \end{bmatrix} \tag{24}$$

Furthermore the equations for the components of permanent magnet and the hollow crank are modeled as a disk, which only characterized by its kinetic energy. The node of the rotor has four degrees of freedom: two displacements u and w and two slopes about the x-y and y-z planes, which are θ and ψ respectively. Then if the nodal displacement vector δ of center of the disk is

$$\delta = [u, w, \theta, \psi]^T \tag{25}$$

By applying the Lagrange equations, the equation for the disk:

$$\frac{d}{dt}\left(\frac{\partial T}{\partial \dot{\delta}}\right) - \frac{\partial T}{\partial \delta} = \begin{bmatrix} M_D & 0 & 0 & 0 \\ 0 & M_D & 0 & 0 \\ 0 & 0 & I_{Dx} & 0 \\ 0 & 0 & 0 & I_{Dx} \end{bmatrix}\begin{bmatrix} \ddot{u} \\ \ddot{w} \\ \ddot{\theta} \\ \ddot{\psi} \end{bmatrix} + \Omega\begin{bmatrix} 0 & 0 & 0 & 0 \\ 0 & 0 & 0 & 0 \\ 0 & 0 & 0 & -I_{Dy} \\ 0 & 0 & I_{Dy} & 0 \end{bmatrix}\begin{bmatrix} \dot{u} \\ \dot{w} \\ \dot{\theta} \\ \dot{\psi} \end{bmatrix} \tag{26}$$

where the first matrix is the classical stiffness matrix and the second one is the matrix due to gyroscopic effects.

In this study, the effects of unbalanced mass and bearing influence are neglected so that the general equation of rotor dynamics is

$$M\ddot{\delta} + K\delta = F(t) \tag{27}$$

where δ is all nodal displacement vectors, M is the mass matrix, K is the stiffness matrix and $F(t)$ is the force vector.

1D finite element analysis in this study uses the discretization of 4 elements and 5 nodal. Simplification scheme of the rotor with dimension in mm is shown in Figure 3.

To produce the equality throughout the element, the local element matrix of each element is arranged into a global matrix. Every element, which has the same number of nodal and that of degrees of freedom, is placed on the same row and column and this applies to the mass matrix, stiffness matrix and damping matrix [14]. The
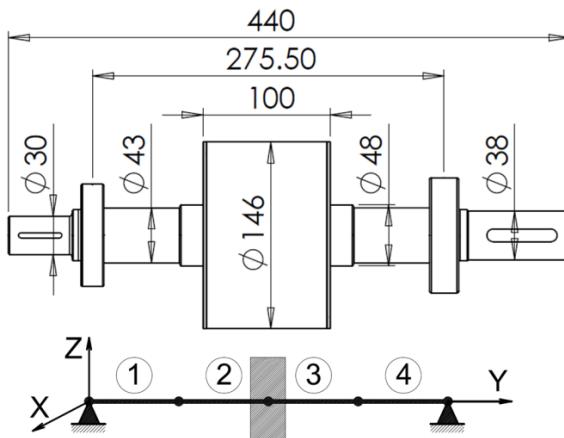
Figure 3. Simplification scheme of the discretization in 1D finite element analysis for the rotor

B. 3D Finite Element

The evaluation procedures of 3D finite element analysis using ANSYS to analyze rotor-dynamic characteristics consist of geometric modeling, material definition, meshing (discretization), the determination of boundary conditions, calculation, and displaying the results [6][7]. In the geometry modeling stage, the geometry of every rotor component is made in 3D and its material type is defined from specification. Meshing stage is conducted by dividing the components into small elements with a finite number and then doing analysis according to the material properties, boundary conditions and loading. In this study, the tetrahedral 3D element type on auto-mode is used, meaning that the discretization step is performed automatically by ANSYS program, including the selection of the elements number. After the processes of iteration and calculation are solved, then the final stage is to display the results of the simulation.

illustrative example of the element assembly from local elements into global element for two local elements can be seen in Figure 4. Globalizing matrix in this way is the fastest and easy, even for a lot of elements and nodal degrees of freedom. In addition to the dimensions of each component of the rotor, the mechanical properties of the component are also required as the input data of the calculation. In this study, the material of the shaft is JIS S45C steel, with Poissons ratio v = 0.27 to 0.30, tensile strength = 569 MPa, yield strength = 343MPa, Young's modulus, E = 190 to 210 GPa and density = 7,700 to 8,030 kg/m^3 [16]. Meanwhile, the disk consists of two components, namely the crank is made of steelST37 and the permanent magnet type is NdFeB. Both the density of the material is almost the same which is about 8,000 kg/m^3.
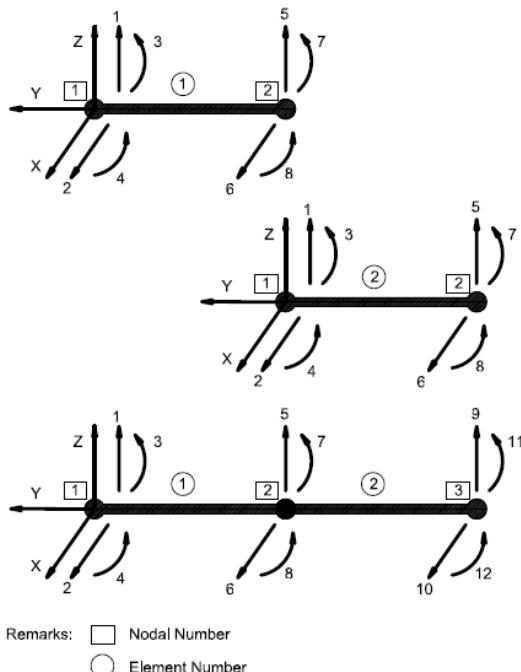
III. RESULTS AND DISCUSSION

A. 1D Finite Element

Campbell diagram showing the output results of numerical simulations using the finite element method represents a natural frequency as a function of rotational speed. Figure 5 shows the dynamic characteristics of the rotor using 1D finite element that are visualized by Campbell diagram, where the X axis is the rotation in rpm and the Y axis is the natural frequency of the system. The black solid line indicates the frequency of the rotor which equals to the frequency of rotation, while the black dashed line indicates the frequency of the rotor which equals half of the frequency of the rotation.

Figure 4. Element assembly from local elements into global element for two elements [15][16]
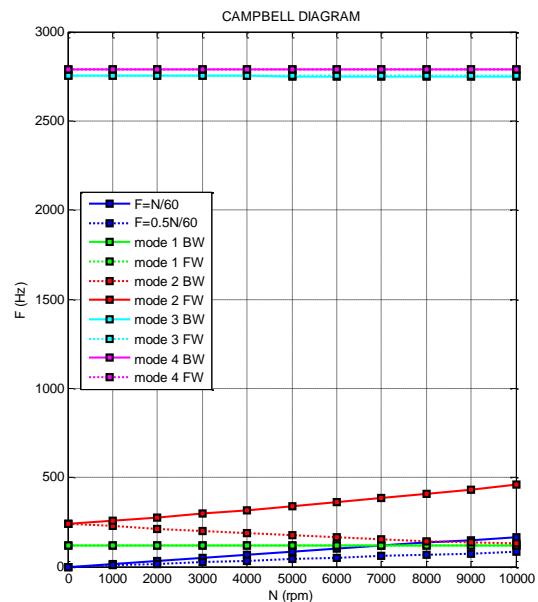

Figure 5.Campbell diagram of 1D finite element analysis

The simulation results illustrate only the first four modes in the diagram because the value of the other modes is far above the operating speed of the motor. Each mode has two lines of response in the opposite direction those are FW (solid line) and BW (dashed line). When the response lines equal to the rotational speed or showing intersections in the diagram then these intersections are called critical speed. The maximum speed of the IPM motor refers to the maximum frequency of the speed control used that is 300 Hz. Having 6 poles number, the maximum speed of the motor equals to 120 multiplied by the frequency and divided by the number of poles yields 6,000 rpm. According to the simulation results, the possibilities of rotor critical speeds are in mode 1 and 2, therefore the analysis is focused on both frequencies.

By enlarging the Campbell diagram near the maximum design frequency of 300Hz, modes 1 and 2 are investigated as shown in Figure 6.As shown on Figure 6, there is intersecting point between the response line and mode 1 at the rotational speed of 7,000 rpm (116.4 Hz). However, that critical speed resulted from the 1D finite element analysis is above the motor maximum speed of 6,000 rpm and frequency of 300 Hz so that the motor can operate safely. These results are then compared with the results obtained from 3D finite element analysis.

B. 3D Finite Element

Discretization or meshing in ANSYS uses tetrahedral 3D element in auto mode. The meshing process produces 18,077 elements and 37,571 nodal, shown in Figure 7. If we compared with 1D finite element, that has very few elements and nodal, 3D finite element will
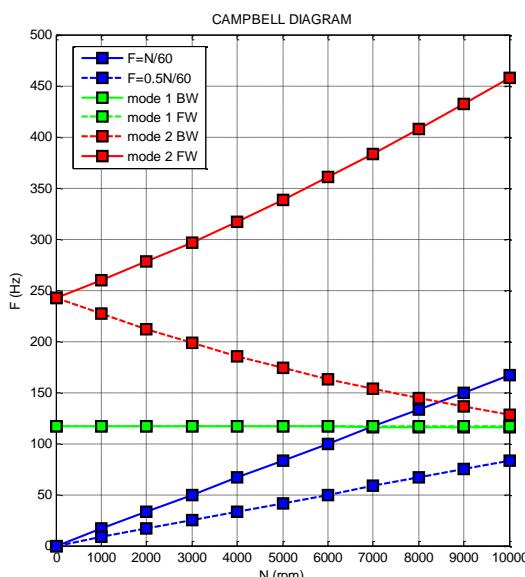
Table 1.
Frequencies at the first ten modes

Mode	Frequency (Hz)
1	505.08
2	552.16
3	655.71
4	992.08
5	1,084.80
6	1,087.40
8	3,288.90
9	3,684.30
10	3,711.70

generate a more detailed analysis on each segment of the rotor.

After iteration and calculation process are solved by the computer, Campbell diagram and each natural frequency modes will be generated from the results of calculations. In this study, the first ten modes are examined and represented in Table 1. From the 10 modes generated by 3D finite element, the smallest natural frequency is well above the design frequency of 300 Hz.

Campbell diagram in Figure 8 shows that all modes do not indicate critical speeds in the system for the rotational velocity 1,000 rad/s or 9,554.14 rpm. Based on these results, the IPM motor designed with the maximum speed of 6,000 rpm and the frequency of 300 Hz can be operated safely. The other simulation result is the modal map in different modes.

The modal maps of the first six modes are shown in Figure 9. The first and the second modes appear to be bending on the disk to the shaft position, while the third and fourth modes there is a shift toward the disk position to the shaft axis. Then at the fifth and sixth modes, bending occurs on the shaft.

IV. CONCLUSION

Rotor-dynamic characteristics of the IPM motor in the form of the critical speed in the Campbell diagram has been evaluated using the 1D and 3D finite element method. 1D finite

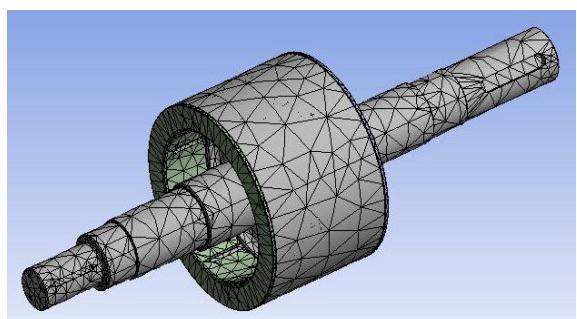Figure 6. Rotor critical speeds in mode 1 and 2

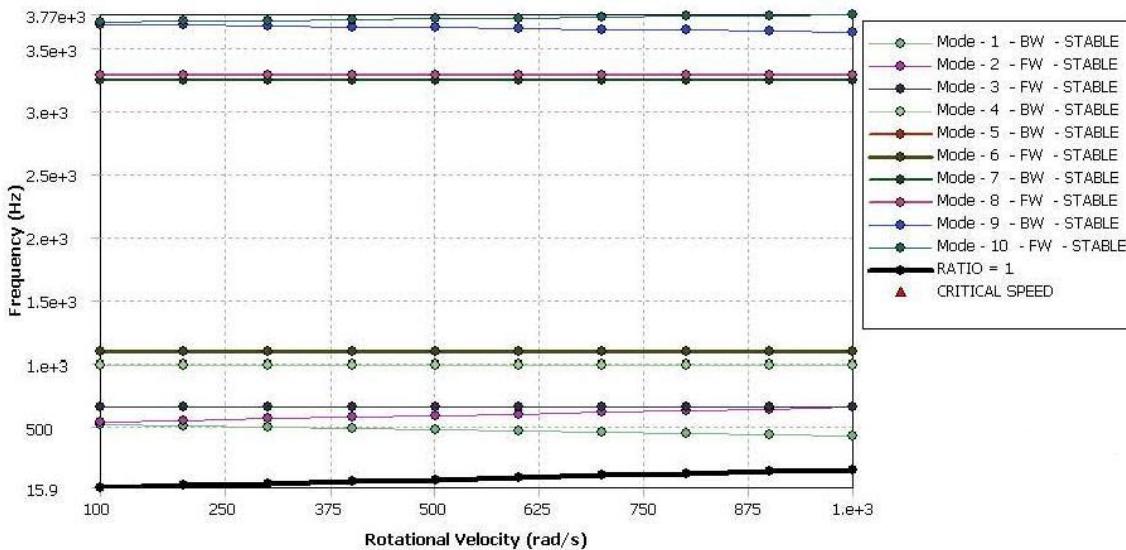Figure 7. Discretization using tetrahedral elements

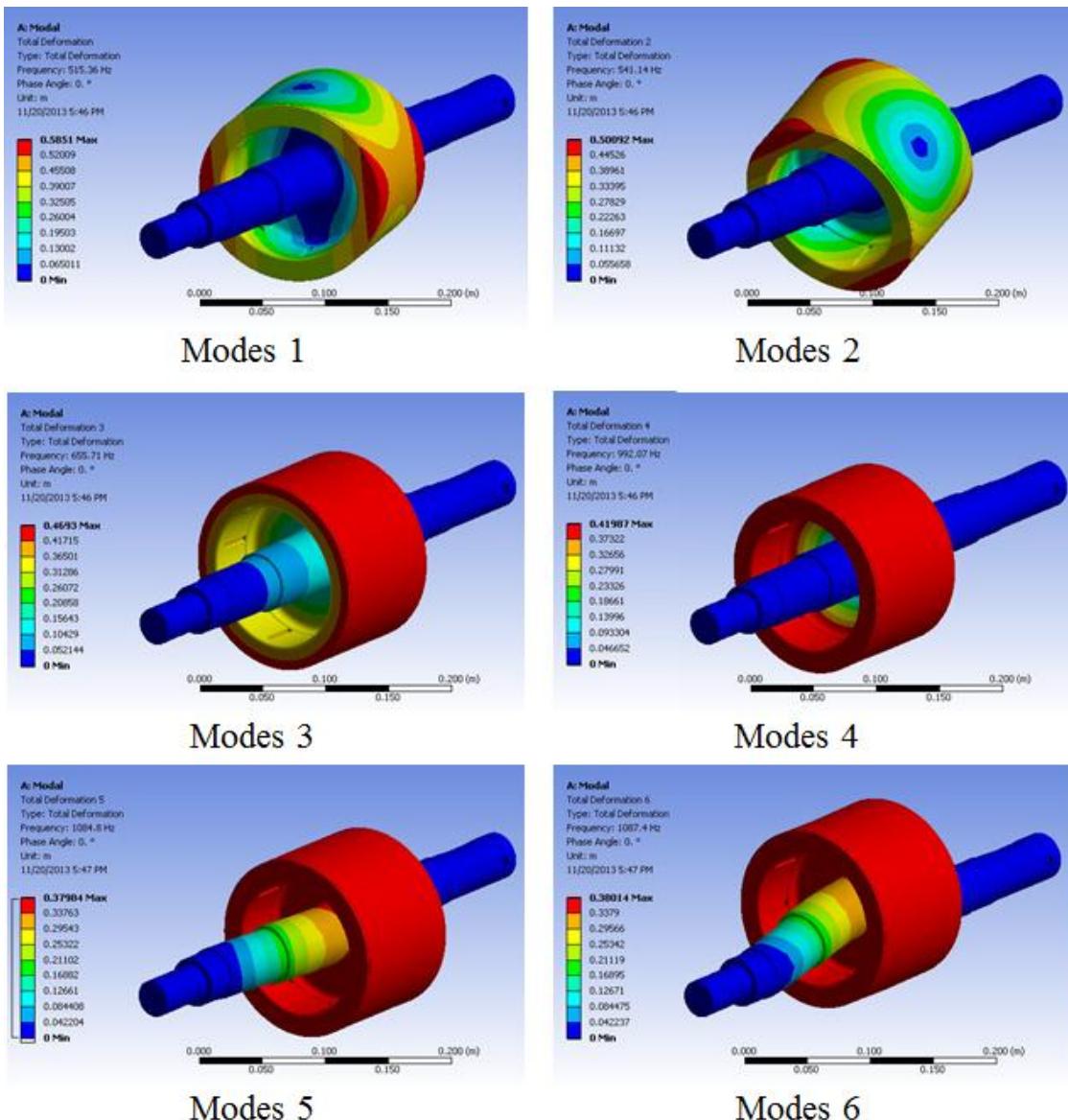Figure 8. Campbell diagram of 3D finite element analysis

Figure 9. The model maps of the first six modes

element analysis yields two modes (modes 1 and 2) which are in the range of frequency design of 300 Hz, however the critical rotational velocity in both modes are still far above the maximum velocity design of 6,000 rpm.

Validation using 3D finite element analysis demonstrates that all modes are still above of the designed frequency and did not find any critical speeds below 6,000 rpm. It can be concluded that the critical speed of the rotor of IPM motor is still outside the system resonance region and could be operated safely.

ACKNOWLEDGEMENT

REFERENCES

[1] C. Y. Young, *et al.*, "Research on the Output Characteristics of IPMSM according to the Pole-Slot Combinations," *Energy Precedia*, Vol. 14, pp. 1187-1192, 2012.
[2] H. M. Hasanien, "Torque Ripple Minimization of Permanent Magnet Synchronous Motor using Digital Observer Controller," *Energy Conversion and Management*, Vol. 51, pp. 98-104, 2010.
[3] C.C. Hwang, *et al.*, "Comparison of Performances Between IPM and SPM Motors with Rotor Eccentricity," *Journal of Magnetism and Magnetic Materials*, Vol. 282, pp. 360-363, 2004.
[4] J. D. Ede, *et al.*, "Rotor Resonances of High-Speed Permanent-Magnet Brushless Machines," *IEEE Transactions on Industry Applications*, Vol. 38, No. 6, pp. 1542-1548, 2002.
[5] S. I. Kim, *et al.*, "Optimization for Reduction of Torque Ripple in Interior Permanent Magnet Motor by Using the Taguchi Method," *IEEE Transactions on Magnetics*, Vol. 41, No. 5, pp. 1796-1799, 2005.
[6] F. Trebuňa1, *et al.*, "Numerically Computed Dynamics Rotor using Ansys Software," *The 4th International Conference: Modelling of Mechanical and Mechatronic systems*, Herľany, Slovak Republic, pp. 498-501, 2011.
[7] B. Bai, *et al.*, "Analysis of Dynamic Characteristics of the Main Shaft System in a Hydro-turbine Based on ANSYS," *Procedia Engineering*, Vol. 31, pp. 654-658, 2012.
[8] H. Taplak and M. Parlak, "Evaluation of Gas Turbine Rotor Dynamic Analysis using the Finite Element Method," *Measurement*, Vol. 45, pp. 1089-1097, 2012.
[9] I. Bucher and D. J. Ewin, "Modal Analysis and Testing of Rotating Structures," *Philosophical Transactions - The Royal Society London,* Vol. 359, pp. 61-96, 2001.
[10] M. Chouksey, *et al.*, "Modal Analysis of Rotor-Shaft System under the Influence of Rotor-Shaft Material Damping and Fluid Film Forces," *Mechanism and Machine Theory*, Vol. 48, pp. 81-93, 2012.
[11] P. Paolaor, *et al.*, "Studies of Mechanical Vibrations and Current Harmonics in Induction Motors Using Finite Element Method," *WSEAS Transactions on Systems*, Issue 3, Vol. 7, pp. 195-202, 2008.
[12] Hilman S. Alam, *et al.*, "Analytical and Numerical Deflection Study on the structure of 10 kW Low Speed Permanent Magnet Generator," *Mechatronics, Electrical Power, and Vehicular Technology,* Vol. 03, pp. 87-94, doi: 10.14203/j.mev.2012.v3.87-94, 2012.
[13] Hutton, D. V., *Fundamental of Finite Element Analysis*, USA: The McGraw Hill Company, 2004, pp. 1-50.
[14] Rao S. S., "The Finite Element Method in Engineering 4th Edition," *Elsevier Science*, 2004.
[15] M. Lalanne, G. Ferraris, *Rotor dynamics Prediction in Engineering*, 2nd Edition, United Kingdom: John Wiley and Sons Ltd, 1998, pp. 1-248.
[16] T. Admono, (2003), "Pembuatan Program Simulasi Prediksi Prilaku Dinamik Sistem Mono rotor Menggunakan Matlab," *Pusat Penelitian Informatika LIPI,.* [online]. Available: http://digilib.informatika.lipi.go.id/informatika/mybox/290tri_admono_pembuatan_program_simulasi_monorotor.pdf.
[17] JIS S45C Mild Steel an Overview, *Mead Info*, 2010. [online]. Available: http://www.meadinfo.org/2010/03/s45c-jis-mechanical-properties.htm